frontiers | Frontiers in Chemistry

Check for updates

Thermal mechanism in magneto radiated [(Al$_2$O$_3$-Fe$_3$O$_4$)/blood]$_{hnf}$ over a 3D surface: Applications in Biomedical Engineering

Kamel Guedri[1], Adnan[2]*, Zehba Raizah[3,4], Elsayed Tag Eldin[5], M. A. EL-Shorbagy[6,7], Waseem Abbas[2] and Umar Khan[8]

[1]Mechanical Engineering Department, College of Engineering and Islamic Architecture, Umm Al-Qura University, Makkah, Saudi Arabia, [2]Department of Mathematics, Mohi-ud-Din Islamic University, Nerian Sharif, AJ&K, Pakistan, [3]Department of Mathematics, College of Science, King Khalid University, Abha, Saudi Arabia, [4]Research Center for Advanced Materials Science (RCAMS), King Khalid University, Abha, Saudi Arabia, [5]Faculty of Engineering and Technology, Future University in Egypt New Cairo, New Cairo, Egypt, [6]Department of Mathematics, College of Science and Humanities in Al-Kharj, Prince Sattam Bin Abdulaziz University, Al-Kharj, Saudi Arabia, [7]Department of Basic Engineering Science, Faculty of Engineering, Menoufia University, Shebin El-Kom, Egypt, [8]Department of Mathematics and Statistics, Hazara University, Mansehra, Pakistan

Nanofluids are a new generation of fluids which help in improving the efficiency of thermal systems by improving heat transport rate and extensive applications of this class extensively fall in biomedical engineering, the electronics industry, applied thermal and mechanical engineering, etc. The core concern of this study is to examine the interaction of Al$_2$O$_3$-Fe$_3$O$_4$ hybrid nanoparticles of lamina shaped with blood over a 3D surface by impinging novel impacts of non-linear thermal radiations, stretching, velocity slippage, and magnetic field. This leads to a mathematical flow model in terms of highly non-linear differential equations *via* nanofluid-effective characteristics and similarity rules. To know the actual behavior of (Al$_2$O$_3$-Fe$_3$O$_4$)/blood inside the concerned region, mathematical investigation is performed *via* numerical technique and the results are obtained for different parameter ranges. The imposed magnetic field of high strength is a better tool to control the motion of (Al$_2$O$_3$-Fe$_3$O$_4$)/blood inside the boundary layer, whereas, stretching of the surface is in direct proportion of the fluid movement. Furthermore, thermal radiations (Rd) and γ_1 are observed to be beneficial for thermal enhancement for both (Al$_2$O$_3$-Fe$_3$O$_4$)/blood and (Al$_2$O$_3$)/blood.

Introduction

The world of nanotechnology is nothing without the investigation of the dynamics of nano and hybrid fluids (Alharbi et al., 2022). Now-a-days, we see that many researchers have come out with new technological ideas of a hybrid nanofluid, which is an upgraded version of common liquids. Hybrid nanofluids have high thermal conductivity due to the joint contribution of two types of nanoparticles. Therefore, researchers have seriously taken the analysis of such fluids from synthetization to applications and have performed the studies at a high level. Recently, Kashi et al. (Kashi et al., 2020) demonstrated the study of (Cu-Al_2O_3/water) in three dimensions over a slippage surface with uniform surface convection. Another imperative study related to the thermal behavior of Cu-Al_2O_3/water by taking flow assumptions on the surface was conveyed in (Khashi et al., 2020).

The transmission of heat in a hybrid nanoliquid with water as the base component and (Al_2O_3-Cu) hybrid nanoparticles was examined by Zainal et al. (Zaina et al., 2020). The inspection of Lorentz forces in the flow behavior over a 3D surface subject to resistive heating is done in Devi and Devi, 2016a. Hybrid nanofluids are a new generation of heat transport fluids with enriched energy storage ability. Therefore, Devi et al. (Devi and Devi, 2016b) reported a comparative heat transport performance of two nanofluids over a permeable surface. Recently, the stability analysis of (Cu-Al_2O_3/water) (Khan et al., 2022) over a non-linear shrinkable sheet and the heat dynamics under certain physical constraints is described in (Lund et al., 2019). Usman et al. (Usman et al., 2018) studied the significant effects of non-linear thermal radiations (Khan et al., 2021) with the contribution of thermal conductance on the temperature of nanoliquids and explored that the imposition of thermal radiation as an enriched natural source to boost the heat storage ability of the nanoliquids.

The investigation of momentum slippage and MHD (Ahmed, Adnan, and Mohyud-Din, 2020) on Cu-Al_2O_3/water nanofluid flow over a permeable stretching sheet is described in Wahid et al., 2020. Furthermore, a study of nanoliquids influenced by gravity is examined in Jamaludin et al., 2020. A hybrid nanofluid with surface temperature and Lorentz forces was examined by Prakash et al.,2016 and concluded that the hybrid nanofluid had better efficiency than traditional nanofluids. Another significant contribution in thermal enhancement is reported in Colak et al., 2020 to estimate the specific heat of Cu-Al_2O_3/water hybrid nanofluid based on temperature (T) and volume concentrations (φ). Mehryan et al. (Mehryan et al., 2017) studied the free convection thermal performance in a cavity with nanofluids and pointed out that the thermophysical attributes of the nanoparticles empower the thermal transport rate in nanoliquids.

Lund et al. (Lund et al., 2020) explored the thermal characteristics of Cu-Al_2O_3/water by considering MHD and viscous dissipation insights over a shrinkable sheet. Alshare et al. (Alshare et al., 2020) investigated the nano and hybrid nanofluid heat transport mechanisms in a periodic structure and found that enhancing % volume fraction will result increment in the temperature and frictional effects. A numerical analysis of an unsteady MHD mixed convection (Khan, Adnan, and Haleema, 2022) stagnation point flow heat transmission model (SPFM) for Cu-Al_2O_3/water over a 3D oriented geometry is described in Zainal et al., 2021. Nur et al. (Wahid et al., 2020) examined an analytic solution under slip momentum and thermal radiation influences on magnetized Cu-Al_2O_3/water nanofluid over a permeable stretching sheet (Adnan et al., 2022a). Force convection of turbulent flow of pure water, Al_2O_3/water nanofluid, and Cu-Al_2O_3/water hybrid nanofluid through a uniformly heated circular geometry is numerically analyzed in Takabi and Shokouhmand, 2015. Some other beneficial heat transport investigations in nanoliquids are reported in (Roy et al., 2020), (Adnan and Ahmed, 2022), (Leong et al., 2020), (Waqas et al., 2021), (Adnan and Ashraf, 2022a).

Jamshed et al. (Jamshad et al., 2021) studied the Casson nanofluid and examined the results for entropy and heat transport under solar thermal radiations. Sajid et al. (Sajid et al., 2021) studied the second law for a parabolic trough surface collector (PTSC) located inside solar aircraft wings, by taking the homo/heterogeneous reaction. Kashi et al. (Khashi et al., 2021) formulated the model for Cu-Al_2O_3/water hybrid nanofluid using the single-phase technique and reported a detailed analysis. Recent investigations were revealed in the studies by Adnan et al., 2020a, Adnan et al., 2022b, Adnan et al., 2020b, and Ahmed et al., 2017.

The study of electroosmotic silver/water nanoliquids in peristaltic geometry *via* two distinct approaches is done by Akram et al. (Akram et al., 2022a). They treated the developed model through different approaches and analyzed the dynamics due to fluctuating peristalsis parameters. An experimental analysis regarding the resistance of anti-microbes for gold nanoparticles is described by Habib and Akbar (Habib and Akbar, 2021) and the results are explained in a comprehensive manner. The exploration of an exact solution for various fluid dynamic heat transmission models is of great significance to examine the behavior of the temperature inside the concerned region. In this regard, a significant analysis is reported by Akbar et al. (Akbar et al., 2022). The impacts of thermal radiations on the nanoliquid whose components are CNTs and water are explained in detail. The entropy investigation in a new Rabinowitsch nanoliquid due to peristaltic pumping is discussed by Akram et al. (Akram et al., 2022b). Some recent and well-contributed studies in the area of applied fluid mechanics from various physical aspects (thermal radiations, magnetic field, heat sink/source inside the fluid, viscous dissipation, joule heating, etc.) of flow and geometry are elaborated in Akram and Akbar, 2020; Akram et al., 2020; Butt et al., 2020 at various spans of time.
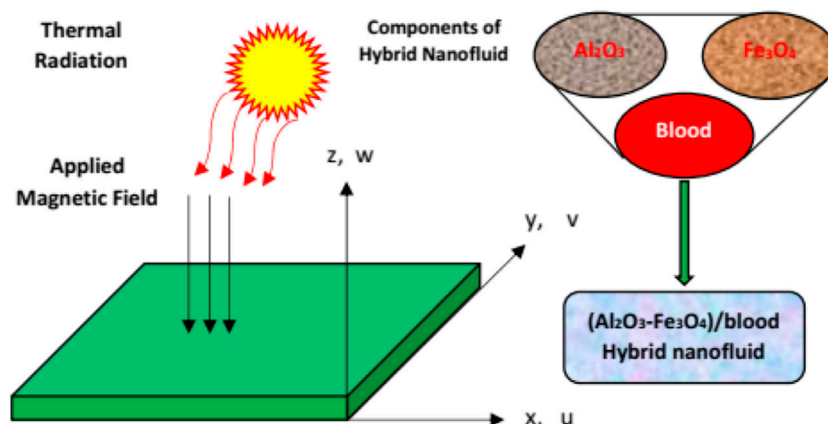
FIGURE 1
The Physical flow configuration of (Al_2O_3-Fe_3O_4)/blood and Al_2O_3/blood.

The dynamics of nanoliquid in a curved channel with a thermophoretic movement are disclosed by Akram et al. (Akram et al., 2022c). The authors determined that higher buoyancy forces strengthened the temperature and facilitated the fluid movement. The temperature due to thermal radiations, resistive heating (Abbasi et al., 2017), and dissipation function in a nanoliquid prepared by gold and blood were analyzed by Sridhar et al. (Sridhar et al., 2022). The magnetic field (Akram et al., 2022d) is an important perspective from an industrial view point and broadly applicable in a variety of industries. Therefore, the researchers made several attempts to inspect the temperature transmission and fluid movement under a variety of nanoliquids by taking the flow in different regimes. Such important studies are described in the Refs. (Akram et al., 2022e; Tripathi et al., 2022), (Saleem et al., 2021), (Javid et al., 2021), and (Tripathi et al., 2021).

Model development

Model statement and geometry

Consider a three-dimensional, steady, laminar flow over a surface with modified slip boundaries. The flow is incompressible and subject to the magnetic field. Furthermore, thermal radiations are also imposed over the surface for better thermal performance of the nanofluids. The x and y axes are designated along the length and width of the stretching sheet, respectively; while the z-direction is taken perpendicular to the sheet. We take u, v, and w, as the velocity components along the x, y, and z directions, respectively. Furthermore, we imposed a magnetic field $\mathbf{B_o}$ with uniform strength and aligned along z-axis. The flow region for the used nanofluids is depicted in Figure 1.

The steady Prandtl boundary layer flow of the nanoliquid can be described by the following PDEs (Devi and Devi, 2016a), (Hayat et al., 2015):

$$\frac{\partial \bar{u}}{\partial x} + \frac{\partial \bar{v}}{\partial y} + \frac{\partial \bar{w}}{\partial z} = 0, \tag{1}$$

$$\bar{u}\frac{\partial \bar{u}}{\partial x} + \bar{v}\frac{\partial \bar{u}}{\partial y} + \bar{w}\frac{\partial \bar{u}}{\partial z} = V_{hnf}\frac{\partial^2 \bar{u}}{\partial x^2} - \frac{\sigma_{hnf}B_o^2 \bar{u}}{\rho_{hnf}}, \tag{2}$$

$$\bar{u}\frac{\partial \bar{v}}{\partial x} + \bar{v}\frac{\partial \bar{v}}{\partial y} + \bar{w}\frac{\partial \bar{u}}{\partial z} = V_{hnf}\frac{\partial^2 \bar{v}}{\partial z^2} - \frac{\sigma_{hnf}B_o^2}{\rho_{hnf}}\bar{v}, \tag{3}$$
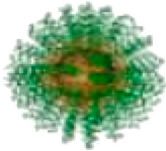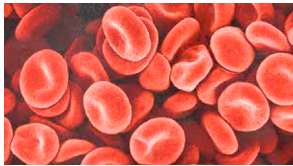
$$\bar{u}\frac{\partial T}{\partial x} + \bar{v}\frac{\partial T}{\partial y} + \bar{w}\frac{\partial T}{\partial z} = \alpha_{hnf}\frac{\partial^2 T}{\partial z^2} + \frac{16\sigma^* T_\infty^3}{3k^*(\rho Cp_{hnf})}\frac{\partial^2 T}{\partial z^2}. \tag{4}$$

The flow on the boundaries is specified to the following rules (Hayat et al., 2015):

$$\left. \begin{cases} \bar{u} = ax + \dfrac{(2-\sigma_v)}{\sigma_v}\lambda_0\dfrac{\partial \bar{u}}{\partial z} \\[2mm] \bar{v} = by + \dfrac{(2-\sigma_v)}{\sigma_v}\lambda_0\dfrac{\partial \bar{v}}{\partial z} \qquad \bar{w} = 0, \\[2mm] \bar{u} \to 0,\ \bar{v} \to 0,\ T \to T_\infty,\ as\, z \to \infty \end{cases} \right\} at\, z = 0 \tag{5}$$

The quantities appearing in the aforementioned governing laws are V_{hnf} (Kinematic viscosity), ρ_{hnf} (Density), k_{hnf} (Thermal conductivity), α_{hnf} (Thermal diffusivity), $\mathbf{B_O}$ (Uniform magnetic field), and a and b are constants representing the stretching surface rate.

TABLE 1 The values for thermophysical attributes and nanoparticle shape factors.

Characteristics	Density ($\frac{\rho g}{m^3}$)	Heat capacity ($\frac{J}{Kg\ K}$)	Thermal conductivity (W/mk)	Electrical conductivity (S/m)
Blood	1063	3594	0.492	4.3×10^{-3}
Al_2O_3	3970	765	40	35×10^6
Fe_3O_4	5180	670	9.7	6.9×10^{-2}
Shape factor values				
Particle's name	Shape	Shape factor vale (n)		
Lamina		16.1576		
Platelets		5.7		
Hexahedron		3.7221		

Thermo-physical attributes for nano and hybrid fluids

The following are thermophysical attributes of nano and hybrid fluids utilized to modify the problem for (Al_2O_3-Fe_3O_4)/blood and Al_2O_3/blood over a desired 3D stretchable surface (Khan et al., 2017; Adnan and Ashraf, 2022b):

$\rho_{nf} = (1-\phi)\rho_s$ (density),

$(\rho C_p)_{nf} = (1-\phi)(\rho C_p)_f + \phi(\rho C_p)_s$ (heat capacity),

$\mu_{nf} = \frac{\mu_f}{(1-\phi)^{2.5}}$ (dynamic viscosity),

$\frac{k_{nf}}{k_f} = (\frac{k_{s1}+(n-1)*k_f-(n-1)*\phi1*(k_f-k_{s1})}{k_{s1}+(n-1)*k_f+\phi1*(k_f-k_{s1})})$ (thermal conductivity),

$\frac{\sigma_{nf}}{\sigma_f} = \frac{(\sigma_{s1}+2*\sigma_f-2*\phi1*(\sigma_f-\sigma_{s1}))}{(\sigma_{s1}+2*\sigma_f+\phi1*(\sigma_f-\sigma_{s1}))}$ (electrical conductivity), And for hybrid nanofluids, the correlations are defined in the following expressions:

$\rho_{hnf} = \{(1-\phi_2)[(1-\phi_1)\rho_f + \phi_1\rho_{s1}]\} + \phi_2\rho_{s_2}$ (density).

$(\rho C_p)_{hnf} = \{(1-\phi_2)[(1-\phi_1)(\rho C_p)_f +\phi_1(\rho C_p)_{s1}]\} + \phi_2(\rho C_p)_{s_2}$ (heat capacity).

$\mu_{hnf} = \frac{\mu_f}{(1-\phi_1)^{2.5}(1-\phi_2)^{2.5}}$ (dynamic viscosity).

$\frac{k_{hnf}}{k_{nf}} = (\frac{k_{s2}+(n-1)*k_{nf}-(n-1)*\phi2*(k_{nf}-k_{s2})}{k_{s2}+(n-1)*k_{nf}+\phi2*(k_{nf}-k_{s2})})$ (thermal conductivity)

And $\frac{k_{nf}}{k_f} = (\frac{k_{s1}+(n-1)*k_f-(n-1)*\phi1*(k_f-k_{s1})}{k_{s1}+(n-1)*k_f+\phi1*(k_f-k_{s1})})$,

Electrical conductivity $\frac{\sigma_{hnf}}{\sigma_{nf}} = (\frac{(\sigma_{s2}+2*\sigma_{nf}-2*\phi2*(\sigma_{nf}-\sigma_{s2}))}{(\sigma_{s2}+2*\sigma_{nf}+\phi2*(\sigma_{nf}-\sigma_{s2}))})$ where, $\frac{\sigma_{nf}}{\sigma_f} = \frac{(\sigma_{s1}+2*\sigma_f-2*\phi1*(\sigma_f-\sigma_{s1}))}{(\sigma_{s1}+2*\sigma_f+\phi1*(\sigma_f-\sigma_{s1}))}$.

In thermal conductivity correlations, n is the nanoparticle shape factor which is equal to 16.1576 (lamina shape). The specific thermophysical attribute values for the nanoparticles and hosting liquid (blood) are described in Table 1 (Ahmed et al., 2018; Hosseinzadeh et al., 2021; Ashraf et al., 2022).

Similarity rules

The following similarity equations are designated to perform the dimensional analysis of the model:

$$\begin{cases} \bar{u} = axF'^{(\eta)} \quad \bar{v} = ayG'^{(\eta)} \\ \bar{w} = -\sqrt{av_f}[F(\eta)+G(\eta)] \\ \eta = z\sqrt{\frac{a}{v_f}} \quad \beta(\eta) = \frac{T-T_\infty}{T_f-T_\infty} \end{cases} \quad (6)$$

FIGURE 2
Implementation process of the technique.
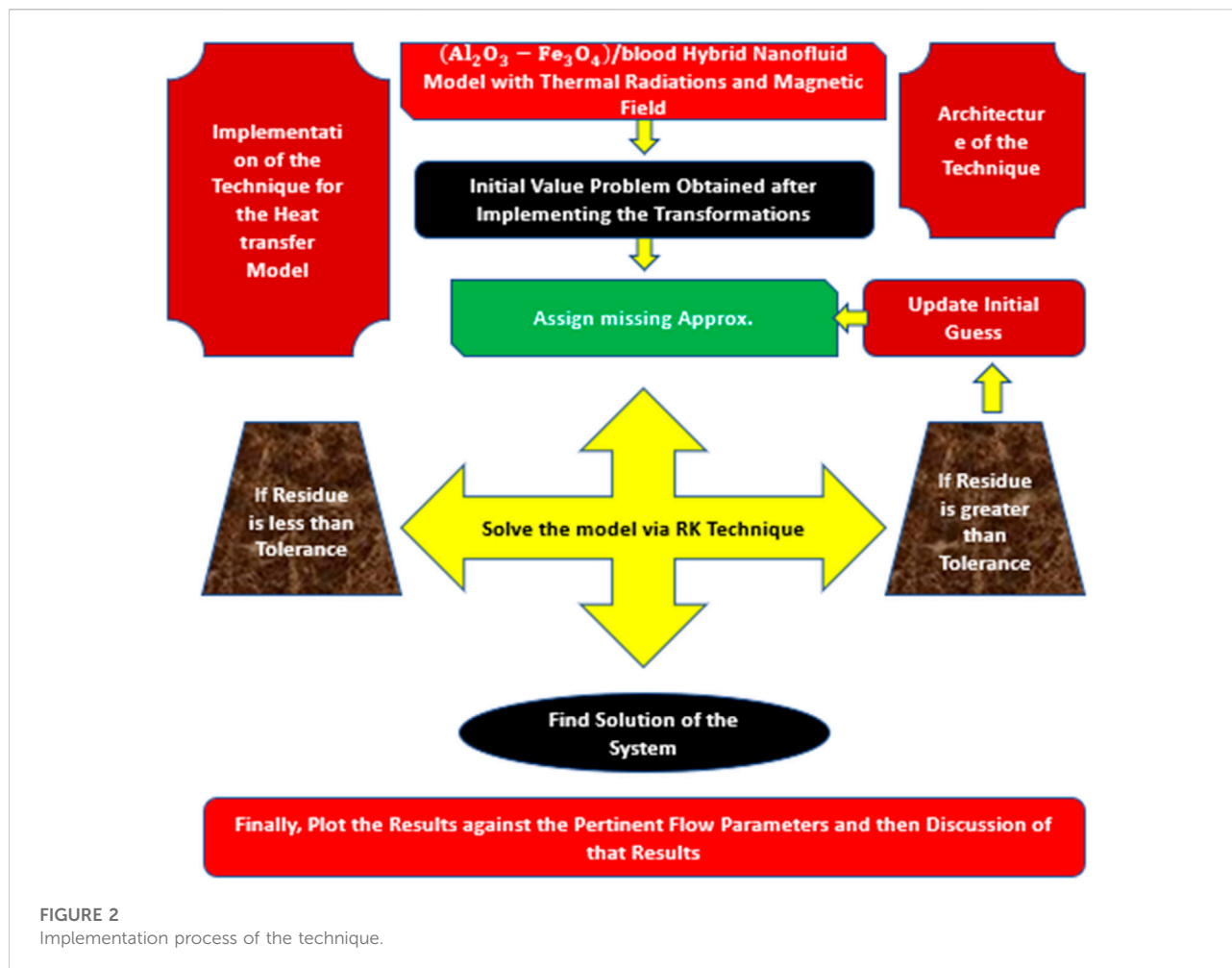
And, the continuity in Eq. 1 is clearly satisfied in the view of aforementioned similarity equations.

Final (Al$_2$O$_3$-Fe$_3$O$_4$)/blood hybrid model

Using similarity transformation and thermo-physical characteristics in the governing model, the final version of the model is achieved:

$$F''' - (1 - \phi_1)^{2.5} (1 - \phi_2) \left\{ (1 - \phi_2) \left[(1 - \phi_1) + \phi_1 \left(\frac{\rho_{s_1}}{\rho_f} \right) \right] \right.$$
$$\left. + \phi_2 \left(\frac{\rho_{s_2}}{\rho_f} \right) \right\} \left[(F')^2 - (G + F) F'' \right]$$
$$- (1 - \phi_1)^{2.5} (1 - \phi_2) M^2 \sigma_{hnf} F'$$
$$= 0, \tag{7}$$

$$G''' - (1 - \phi_1)^{2.5} (1 - \phi_2) \left\{ (1 - \phi_2) \left[(1 - \phi_1) + \phi_1 \left(\frac{\rho_{s_1}}{\rho_f} \right) \right] + \phi_2 \left(\frac{\rho_{s_2}}{\rho_f} \right) \right\}$$
$$\times \left[(G')^2 - (G + F) G'' \right] - (1 - \phi_1)^{2.5} (1 - \phi_2) M^2 \sigma_{hnf} G'$$
$$= 0, \tag{8}$$

$$\beta'' \left(1 + \frac{Rd}{\frac{k_{hnf}}{k_f}} \right) + \frac{Pr}{\frac{k_{hnf}}{k_f}} \left\{ (1 - \phi_2) \left[(1 - \phi_1) + \phi_1 \frac{(\rho C_P)_{s_1}}{(\rho C_P)_f} \right] \right.$$
$$\left. + \frac{\phi_2 (\rho C_P)_{s_2}}{(\rho C_P)_f} \right\} [G + F] \beta'$$
$$= 0, \tag{9}$$

$$\frac{k_{hnf}}{k_f} = \left(\frac{k_{s2} + (n - 1) * k_{nf} - (n - 1) * \phi 2 * (k_{nf} - k_{s2})}{k_{s2} + (n - 1) * k_{nf} + \phi 2 * (k_{nf} - k_{s2})} \right)$$
$$* \left(\frac{k_{s1} + (n - 1) * k_f - (n - 1) * \phi 1 * (k_f - k_{s1})}{k_{s1} + (n - 1) * k_{nf} + \phi 1 * (k_f - k_{s1})} \right),$$
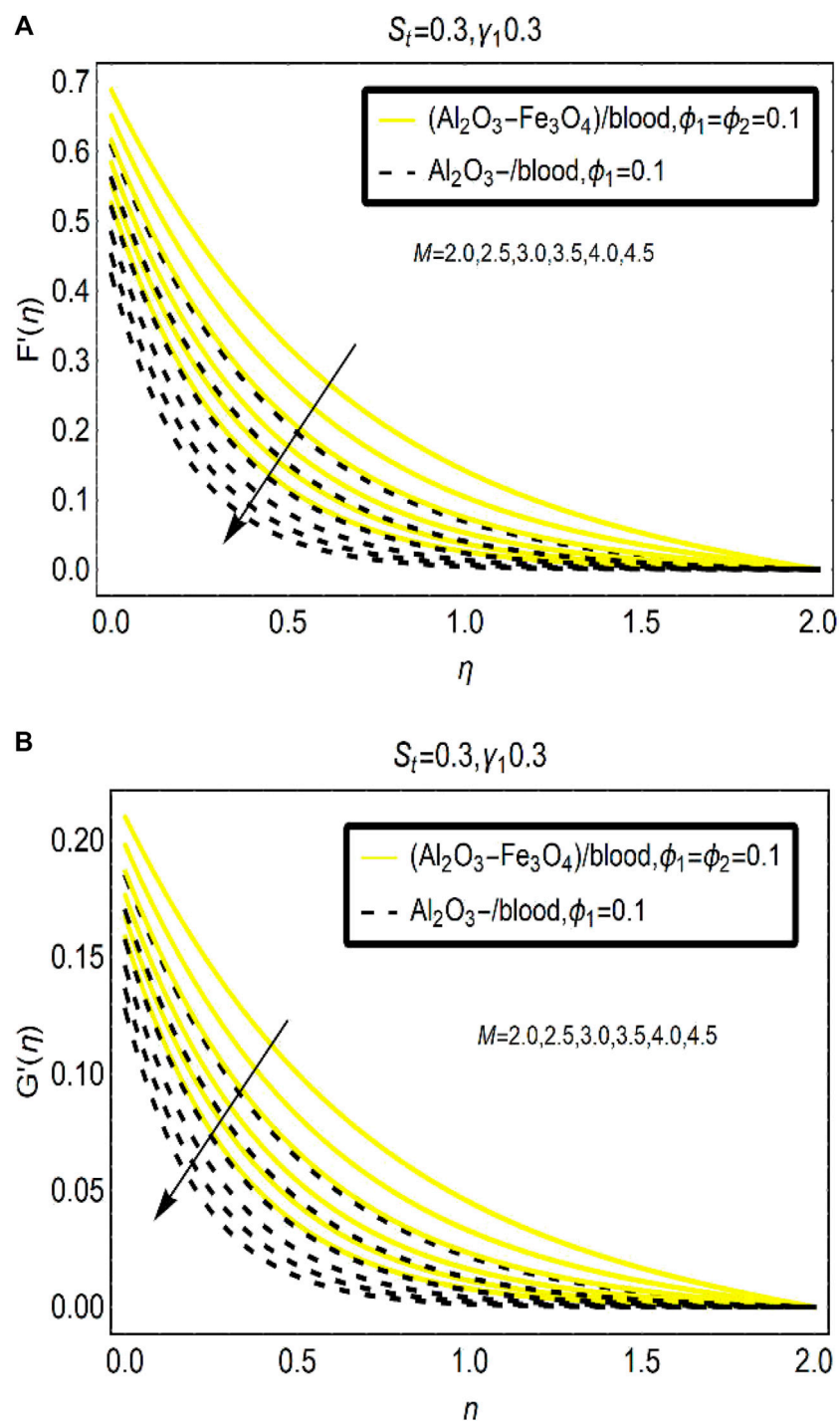
FIGURE 3
The velocity changes under varying M for **(A)** F' and **(B)** G'.

FIGURE 4
The velocity changes under varying γ_1 (slip parameter) for **(A)** F' and **(B)** G'.

$$\sigma_{hnf} = \left(\frac{\left(\sigma_{s2} + 2*\sigma_{\mathrm{nf}} - 2*\phi 2*(\sigma_{\mathrm{nf}} - \sigma_{s2})\right)}{\left(\sigma_{s2} + 2*\sigma_{\mathrm{nf}} + \phi 2*(\sigma_{\mathrm{nf}} - \sigma_{s2})\right)} \right)$$
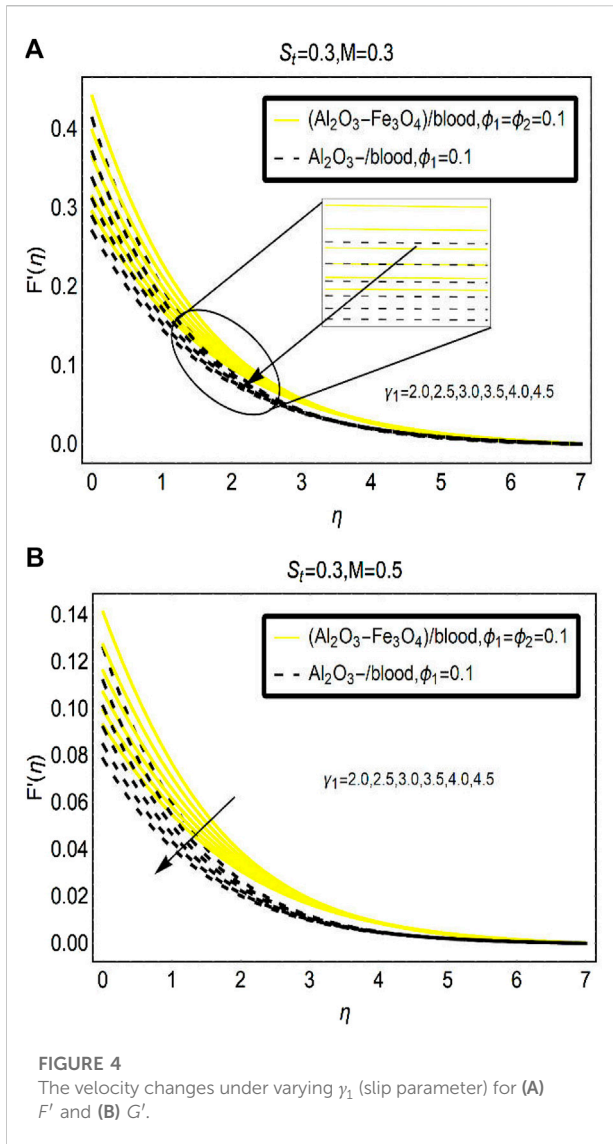$$* \left(\frac{\left(\sigma_{s1} + 2*\sigma_f - 2*\phi 1*(\sigma_f - \sigma_{s1})\right)}{\left(\sigma_{s1} + 2*\sigma_f + \phi 1*(\sigma_f - \sigma_{s1})\right)} \right)$$

With the boundary conditions,

$$\begin{cases} F'(0) = 1 + \gamma_1 F''(0), \quad G'(0) = S_t + \gamma_1 G''(0), \quad [F(0) + G(0)] = 0, \\ \qquad\qquad\qquad \beta(0) = 1, \\ \quad F'(\infty) \to 0, \quad G'(\infty) \to 0, \quad \beta(\infty) \to 0, \end{cases}$$

$$(10)$$

Furthermore, $S_t = b/a$ (stretching parameter), $M^2 = \sigma B_0^2 / a\rho_f$ is the magnetic interaction parameter, $Rd = 16\sigma^* T_\infty^3 / 3k^* k_f$ is the Radiation parameter, and $\gamma_1 = \frac{(2-\sigma_v)}{\sigma_v} \lambda_0 \sqrt{a\nu_f^{-1}\lambda_0}$ (slip parameter).

The skin-friction coefficient C_f, and reduced Nusselt number Nu_x, are defined as:
$$C_f = \frac{\mu_{hnf} \, (\partial u/\partial z)_{z=0}}{\rho_f u_w^2} \text{ and } Nu_x = -\frac{x k_{hnf} \, (\partial T/\partial z)_{z=0}}{k_f \, (T_f - T_\infty)}, \text{ respectively.}$$

Mathematical analysis

The problem in hand is solved numerically due to the high strength of the non-linear terms and it is followed by the following steps:

- Firstly, write the model in its appropriate form.
- Make substitutions according to the order of model.
- Using those substitutions, the higher-order model should be transformed into first order IVP.
- Adjust the BCs accordingly and set those conditions equal to unknowns which will be determined latter.
- Finally, run the code and plot the results for various physical constraints.

The complete working rules for Runge-Kutta scheme are given in Figure 2.

By following the flow chart, the model $(Al_2O_3\text{-}Fe_3O_4)$/blood adjust in the following pattern:

$$F''' = (1 - \phi_1)^{2.5} (1 - \phi_2) \left\{ (1 - \phi_2) \left[(1 - \phi_1) + \phi_1 \left(\frac{\rho_{s_1}}{\rho_f} \right) \right] \right.$$
$$\left. + \phi_2 \left(\frac{\rho_{s_2}}{\rho_f} \right) \right\} \left[(F')^2 - (G + F)F'' \right]$$
$$+ (1 - \phi_1)^{2.5} (1 - \phi_2) M^2 \sigma_{hnf} F'$$

$$(11)$$

$$G''' = (1 - \phi_1)^{2.5} (1 - \phi_2) \left\{ (1 - \phi_2) \left[(1 - \phi_1) + \phi_1 \left(\frac{\rho_{s_1}}{\rho_f} \right) \right] \right.$$
$$\left. + \phi_2 \left(\frac{\rho_{s_2}}{\rho_f} \right) \right\} \left[(G')^2 - (G + F)G'' \right]$$
$$+ (1 - \phi_1)^{2.5} (1 - \phi_2) M^2 \sigma_{hnf} G',$$

$$(12)$$

$$\beta'' = \frac{1}{\left(1 + \frac{Rd}{\frac{k_{hnf}}{k_f}}\right)} \left[-\frac{Pr}{\frac{k_{hnf}}{k_f}} \left\{ (1 - \phi_2) \left[(1 - \phi_1) + \phi_1 \frac{(\rho C_p)_{s_1}}{(\rho C_p)_f} \right] \right. \right.$$
$$\left. \left. + \frac{\phi_2 (\rho C_p)_{s_2}}{(\rho C_p)_f} \right\} [G + F]\beta' \right]$$

$$(13)$$

Now according to the model, the following are appropriate transformations:

FIGURE 5
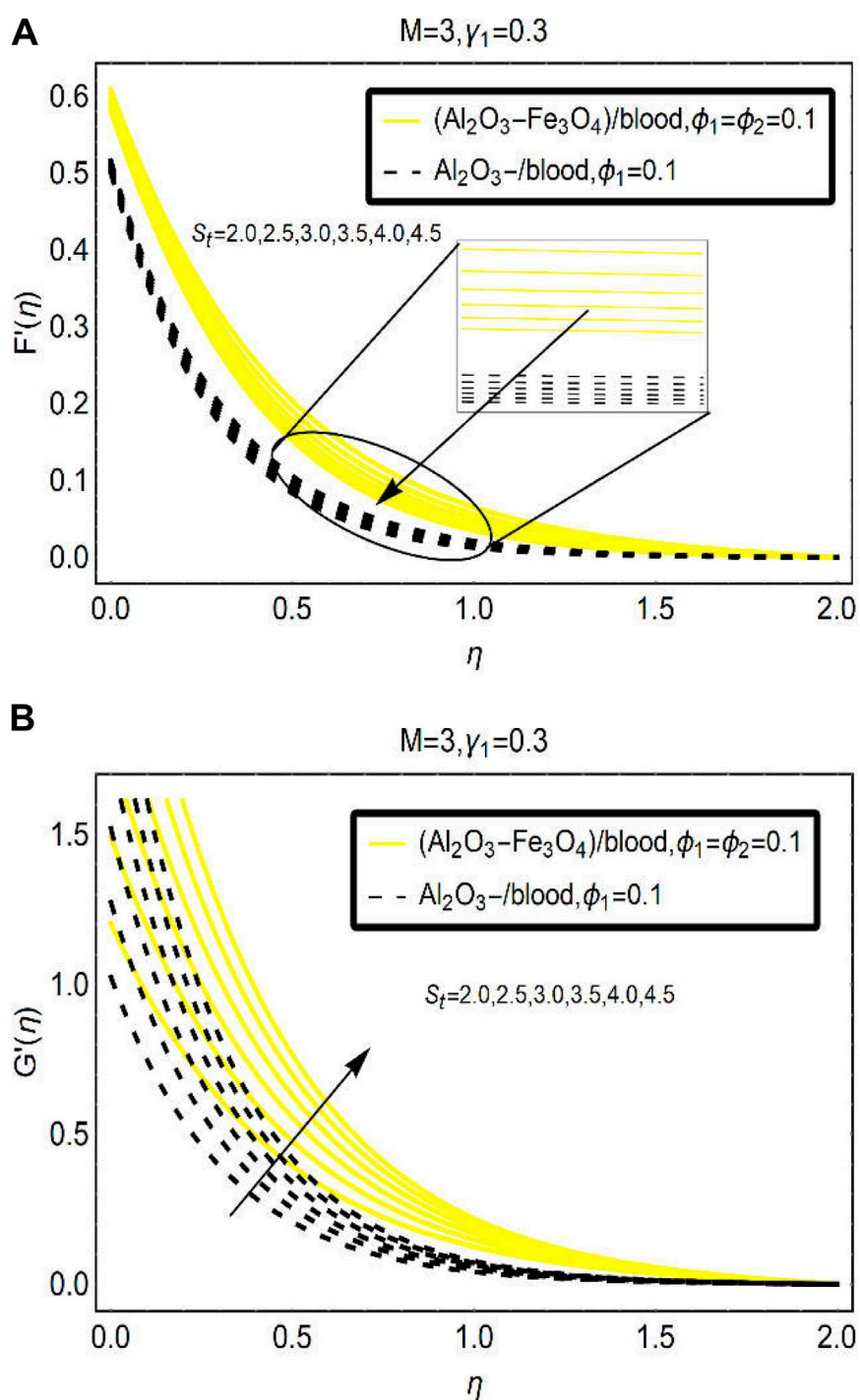The velocity changes under varying S_t (stretching parameter) for **(A)** F' and **(B)** G'.

$$\left[\tilde{\mathfrak{I}}_1 \ \ \tilde{\mathfrak{I}}_2 \ \ \tilde{\mathfrak{I}}_3 \ \ \tilde{\mathfrak{I}}'_3\right]^t = \left[F \ \ F' \ \ F'' \ \ F'''\right]^t$$

$$\left[\tilde{\mathfrak{I}}_4 \ \ \tilde{\mathfrak{I}}_5 \ \ \tilde{\mathfrak{I}}_6 \ \ \tilde{\mathfrak{I}}'_6\right]^t = \left[G \ \ G' \ \ G'' \ \ G'''\right]^t$$

$$\left[\tilde{\mathfrak{I}}_7 \ \ \tilde{\mathfrak{I}}_8 \ \ \tilde{\mathfrak{I}}'_8\right]^t = \left[\beta \ \ \beta' \ \ \beta''\right]^t$$

Eqs 11–13 are then combined in the following form:

$$\tilde{\mathfrak{I}}_3 = (1-\phi_1)^{2.5}(1-\phi_2)\left\{(1-\phi_2)\left[(1-\phi_1)+\phi_1\left(\frac{\rho_{s1}}{\rho_f}\right)\right]\right.$$
$$\left. + \phi_2\left(\frac{\rho_{s2}}{\rho_f}\right)\right\}\left[(\tilde{\mathfrak{I}}_2)^2 - (\tilde{\mathfrak{I}}_1+\tilde{\mathfrak{I}}_4)\tilde{\mathfrak{I}}_3\right]$$
$$+ (1-\phi_1)^{2.5}(1-\phi_2)M^2\tilde{\mathfrak{I}}_2\sigma_{hnf},$$

$$\tilde{\mathfrak{I}}_6 = (1-\phi_1)^{2.5}(1-\phi_2)\left\{(1-\phi_2)\left[(1-\phi_1)+\phi_1\left(\frac{\rho_{s1}}{\rho_f}\right)\right]\right.$$
$$\left. + \phi_2\left(\frac{\rho_{s2}}{\rho_f}\right)\right\}\left[(\tilde{\mathfrak{I}}_5)^2 - (\tilde{\mathfrak{I}}_1+\tilde{\mathfrak{I}}_4)\tilde{\mathfrak{I}}_6\right]$$
$$+ (1-\phi_1)^{2.5}(1-\phi_2)M^2\tilde{\mathfrak{I}}_5\sigma_{hnf},$$

$$\tilde{\mathfrak{I}}_8 = \frac{1}{\left(1+\frac{Rd}{\frac{k_{hnf}}{k_f}}\right)}\left[-\frac{Pr}{\frac{k_{hnf}}{k_f}}\left\{(1-\phi_2)\left[(1-\phi_1)+\phi_1\frac{(\rho C_P)_{s1}}{(\rho C_P)_f}\right]\right.\right.$$
$$\left.\left. + \frac{\phi_2(\rho C_P)_{s2}}{(\rho C_P)_f}\right\} - (\tilde{\mathfrak{I}}_1+\tilde{\mathfrak{I}}_4)\tilde{\mathfrak{I}}_8\right]$$

After this, numerical computation is performed and furnished for the results for various physical constraints over the desired region.

Results and discussion against the physical constraints

The physical flow constraints are imperative to analyze the fluid motion and thermal behavior over a desired region. For the sake of this purpose, the results are organized to examine the hybrid nanofluid dynamics.

The velocity behavior of (Al$_2$O$_3$-Fe$_3$O$_4$)/ blood and Al$_2$O$_3$/blood

Figure 3 demonstrates the velocity of $[(Al_2O_3\text{-}Fe_3O_4)/blood]_{hnf}$ and $[(Al_2O_3)/blood]_{nf}$ against the imposed magnetic field (Figure 3) aligned vertically to the plane of flow. The results reveal that the velocity ($F'(\eta)$ and $G'(\eta)$) of $[(Al_2O_3\text{-}Fe_3O_4)/blood]_{hnf}$ and $[(Al_2O_3)/blood]_{nf}$ drops for the magnetic parameter effects M. Physically, the aligned magnetic field opposes the fluid motion due to which the fluid particles move slowly. In the surroundings of the surface, these
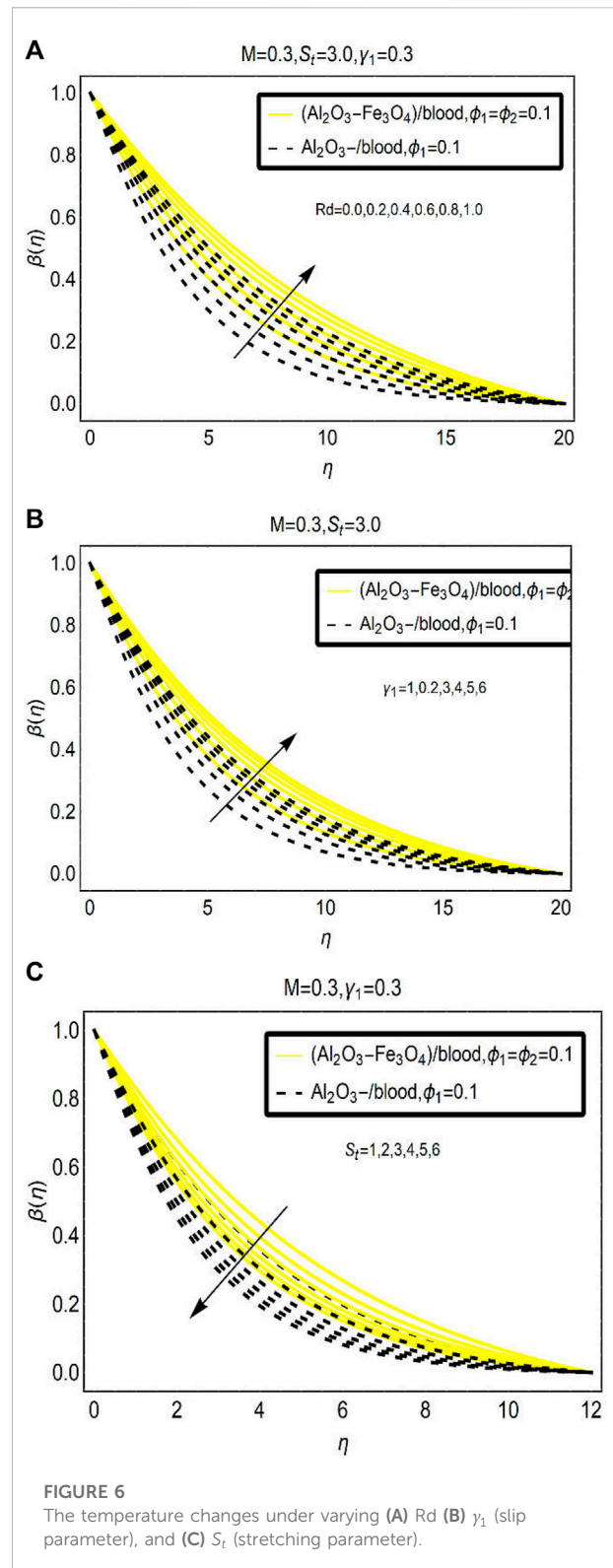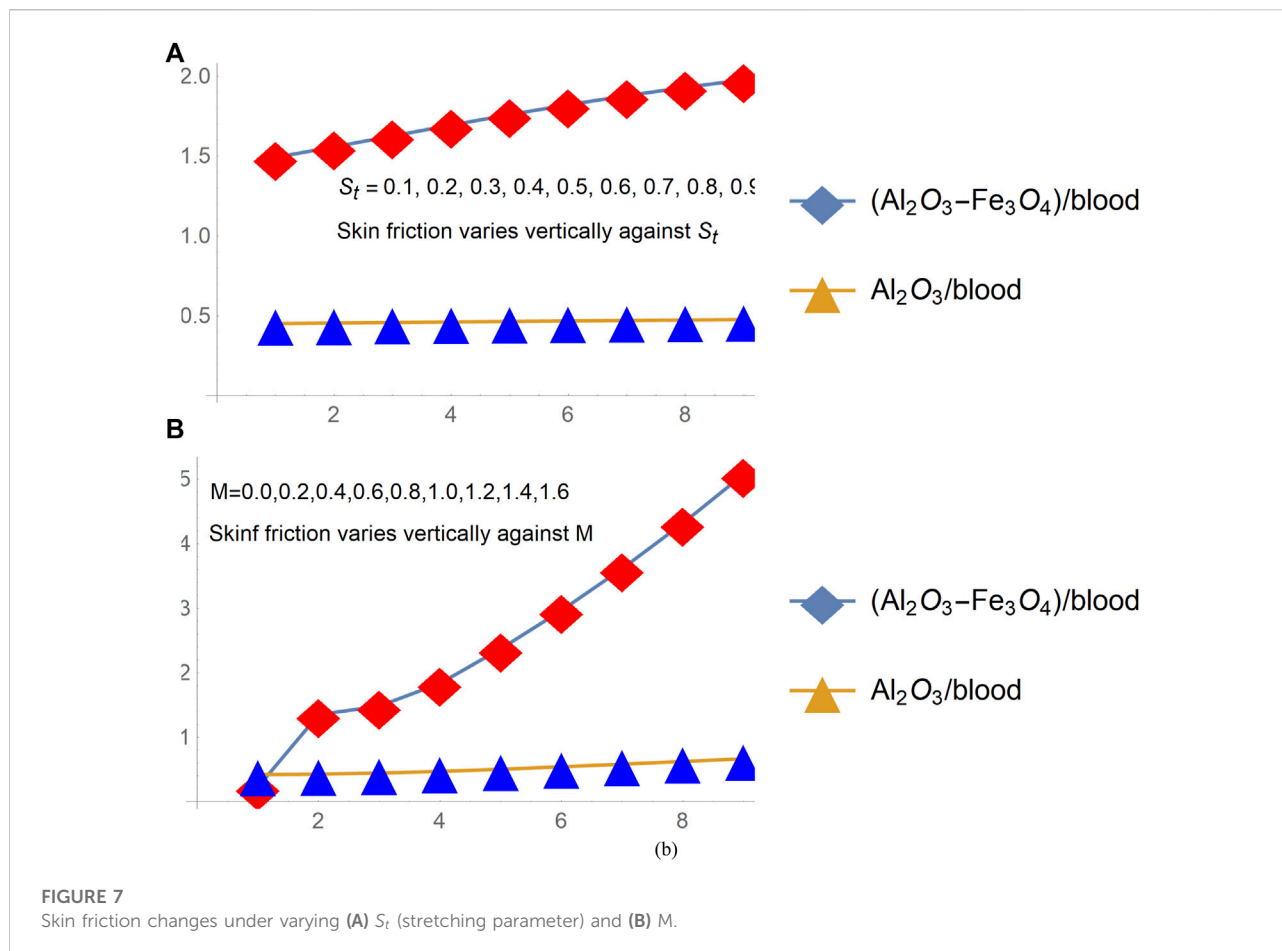

FIGURE 6
The temperature changes under varying **(A)** Rd **(B)** γ_1 (slip parameter), and **(C)** S_t (stretching parameter).

effects are optimum and the motion gradually reduces far from the sheet and finally vanishes at an ambient location from the surface. Thus, the motions of $[(Al_2O_3\text{-}Fe_3O_4)/$

FIGURE 7
Skin friction changes under varying **(A)** S_t (stretching parameter) and **(B)** M.

blood]$_{\text{hnf}}$ and [(Al$_2$O$_3$)/blood]$_{\text{nf}}$ can be controlled by strengthening the aligned magnetic field which is a significant physical phenomena.
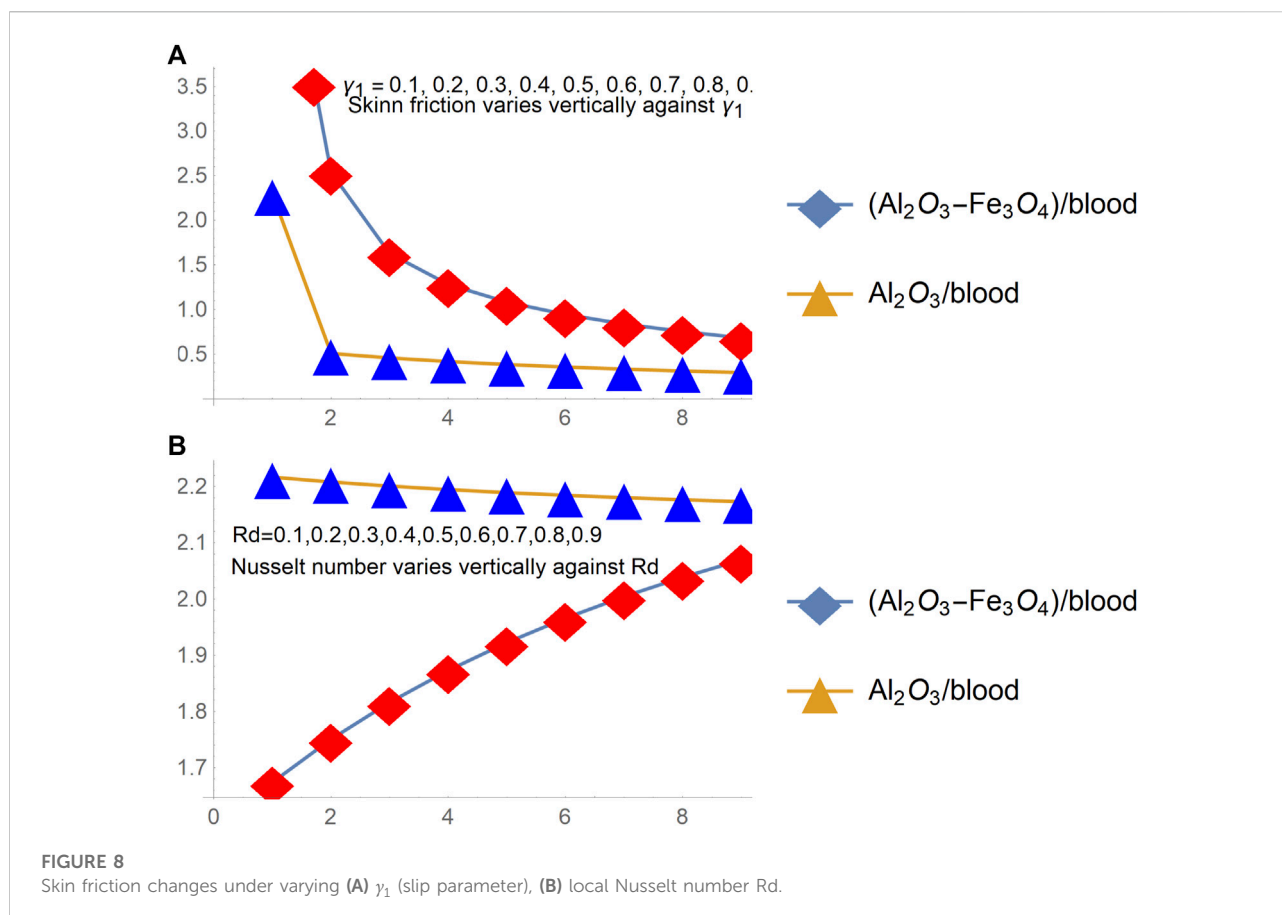
The results for $F'(\eta)$ and $G'(\eta)$ due to a modified slip condition (slip parameter γ_1) at the surface are elaborated in Figure 4. Physically, due to the considered slip effects on the surface, the frictional force reduces between the surface and the immediate fluid layer and in the meanwhile, intermolecular forces playing the role and the fluid movement drops (the densities of the fluid improve due to mono and hybrid nanoparticles). These effects are optimum at the surface due the dominant role of the velocity slip condition and progressively decline at an ambient position. For [(Al$_2$O$_3$-Fe$_3$O$_4$)/blood]$_{\text{hnf}}$, the motion reduces abruptly due to the higher density of the hybrid nanoparticle (Al$_2$O$_3$-Fe$_3$O$_4$). Another physical aspect of this decreasing behavior is the implementation of a magnetic field over the surface.

Stretching of the surface is another physical aspect to observe the fluid movement over the region. Therefore, Figure 5 is furnished to examine the behavior of [(Al$_2$O$_3$-Fe$_3$O$_4$)/blood]$_{\text{hnf}}$ and [(Al$_2$O$_3$)/blood]$_{\text{nf}}$. Very fascinating changes in

the fluid movement are observed due to stretching of the surface. It is explored that the velocity $F'(\eta)$ reduces by increasing the parameter S_t and an almost inconsequential movement of [(Al$_2$O$_3$-Fe$_3$O$_4$)/blood]$_{\text{hnf}}$ and [(Al$_2$O$_3$)/blood]$_{\text{nf}}$ is noticed. However, a significant increment is observed in the velocity $G'(\eta)$ in the surrounding of the sheet. Physically, stretching of the surface enlarges the flowing region over the surface and the [(Al$_2$O$_3$-Fe$_3$O$_4$)/blood]$_{\text{hnf}}$ and [(Al$_2$O$_3$)/blood]$_{\text{nf}}$ particles freely flow over the surface due to which the momentum rises and hence the velocity significantly grows in this region.

Thermal behavior of (Al$_2$O$_3$-Fe$_3$O$_4$)/blood and Al$_2$O$_3$/blood

The analysis of thermal enhancement in [(Al$_2$O$_3$-Fe$_3$O$_4$)/blood]$_{\text{hnf}}$ and [(Al$_2$O$_3$)/blood]$_{\text{nf}}$ is the heart of the study while dealing with nano and hybrid nanofluids. Therefore, a subsequent discussion is about the thermal enhancement in under consideration nanofluid with varying attributes of Rd, γ_1, and S_t. For this, Figure 6 is organized.

FIGURE 8
Skin friction changes under varying **(A)** γ_1 (slip parameter), **(B)** local Nusselt number Rd.
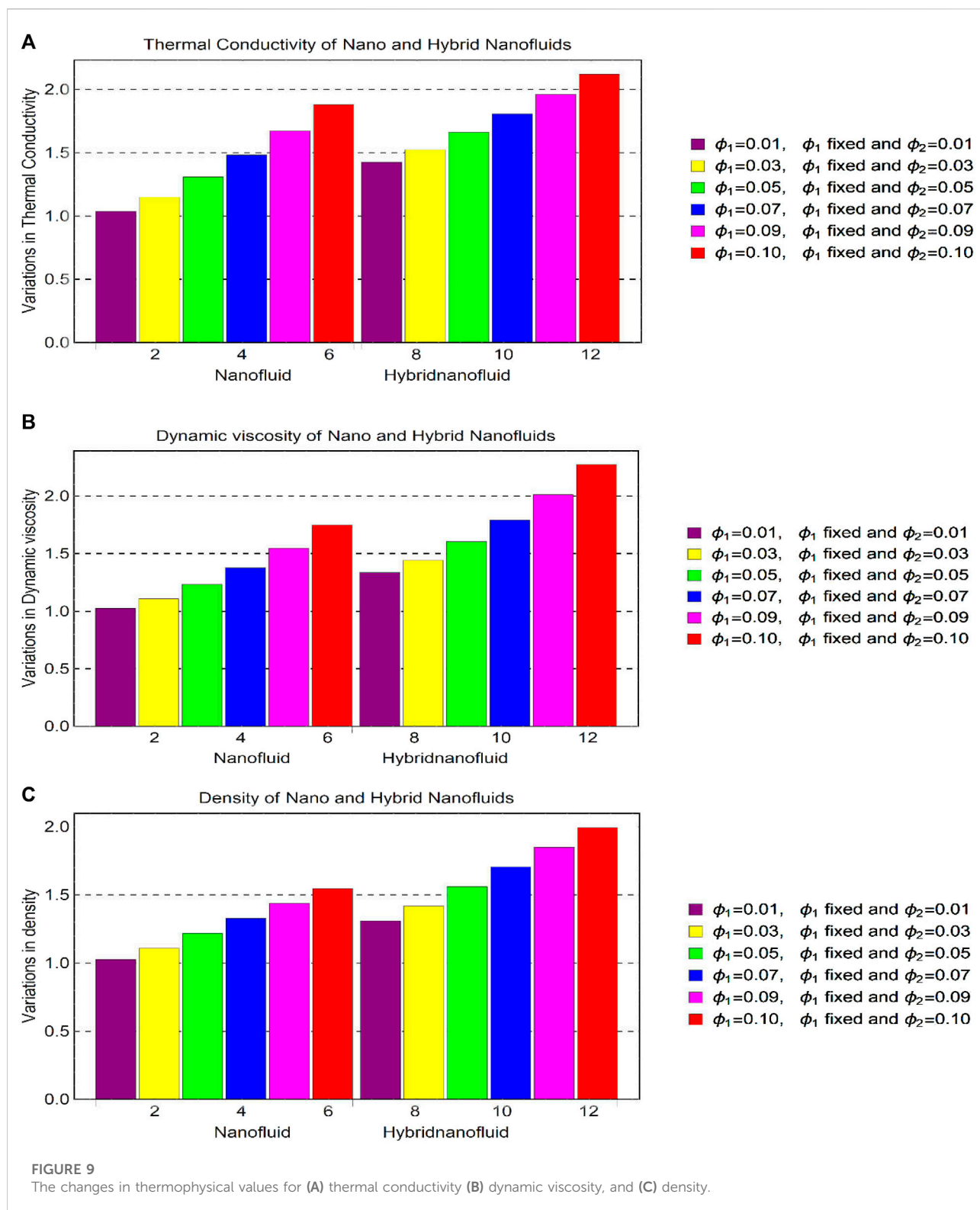
From Figure 6A, it is analyzed that applied thermal radiations over the flow configuration is a very important parameter that significantly alters the temperature characteristics of $[(Al_2O_3\text{-}Fe_3O_4)/blood]_{hnf}$ and $[(Al_2O_3)/blood]_{nf}$ over a stretching radiated surface. Figure 6A discloses that the temperature increases by strengthening the applied thermal radiations (Rd). In $[(Al_2O_3\text{-}Fe_3O_4)/blood]_{hnf,}$ the temperature intensifies rapidly than conventional nanoliquid $[(Al_2O_3)/blood]_{nf}$. Physically, thermal radiations and thermal conductivities of bi and mono nanoparticles in the base solvent (blood) improve thermal storage of the fluid. Therefore, the temperature enhances in both the nanoliquids. In a hybrid nanoliquid, the temperature changes are observed more rapidly than mono nanoliquid due to the difference between their thermal conductivities.

Similarly, Figure 6B and Figure 6C demonstrate the temperature alterations for γ_1 (due to slip BCs) and S_t (due to stretching of the surface), respectively. The implementation of the slip condition became useful for thermal enhancement due to rapid collisions between the fluid particles; whereas, opposing temperature effects are examined in Figure 6C for growing values of surface-stretching parameter S_t.

Quantities of practical interest and thermophysical attributes

The study of skin friction and local heat transport rate achieved much attention of the researchers, and more specifically, engineers because of their significant contribution in various engineering applications. Thus, the behavior of shear stresses and local heat transport rate for $[(Al_2O_3\text{-}Fe_3O_4)/blood]_{hnf}$ and $[(Al_2O_3)/blood]_{nf}$ over a radiated and slippery stretchable surface is pictured in Figures 7, 8, respectively. The parameters of interest in the particular model are the stretching surface ratio (S_t), magnetic number (M), slippery effects (γ_1), and radiation number (Rd).

The analysis of Figure 8 ensures that the shear drag at the slippery surface upturns for a more stretchable and magnetized surface. The rapid growth of shear stresses is inspected for hybrid nanofluid $[(Al_2O_3\text{-}Fe_3O_4)/blood]_{hnf}$ than regular fluid $[(Al_2O_3)/blood]_{nf}$. Being a denser solution, hybrid nanofluid has this characteristic whereas; shear stress decays for growing slippery effects and these are elaborated in Figure 9A. The behavior of the local heat transport rate due to imposed thermal radiation (Rd) is furnished in Figure 9B for both $[(Al_2O_3\text{-}Fe_3O_4)/blood]_{hnf}$ and $[(Al_2O_3)/blood]_{nf}$. The results expose that

FIGURE 9
The changes in thermophysical values for **(A)** thermal conductivity **(B)** dynamic viscosity, and **(C)** density.
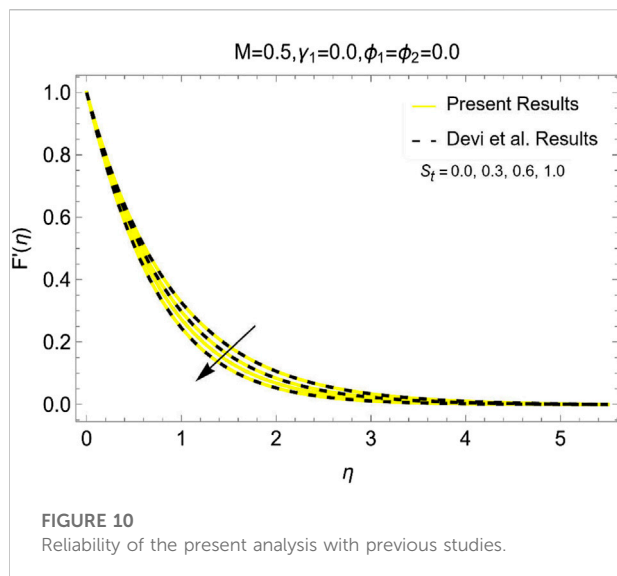
FIGURE 10
Reliability of the present analysis with previous studies.

induction of the thermal radiation in the constitutive model is an important physical aspect to enhance the heat transport rate in nanofluids.

Thermophysical attributes of $[(Al_2O_3\text{-}Fe_3O_4)/blood]_{hnf}$ and $[(Al_2O_3)/blood]_{nf}$ knowingly depend on the thermophysical empirical correlations. Therefore, the behavior of these quantities due to volume fraction is depicted in Figure 9 for thermal conductance, dynamic viscosity, and density. It is inspected that, by the strengthen volume fraction within a reasonable domain, the thermophysical attributes increase which lead to a significant contribution in the nano and hybrid nanoliquids. It is also evident that, due to high thermal conductance of the hybrid nanoparticles, hybrid nanoliquid has much greater ability to store thermal energy.

Code and study of validation

The code and study validation with previously published data is an important factor in numerical investigation. Thus, the results of the model and code are validated with the data of Devi et al. (Devi and Devi, 2016a) by restricting the present model to some flow parameters. The comparative results for altering the stretching parameter (S_t = 0.0, 0.3, 0.6, 1.0) and fixed magnetic strength in Figure 10 are the evidence that the developed code and the results are valid and these can be replicated in the future.

Conclusion

The analysis of $[(Al_2O_3\text{-}Fe_3O_4)/blood]_{hnf}$ and $[(Al_2O_3)/blood]_{nf}$ over a 3D extendable surface is conducted. The heat transport problem formulation is carried out with proper utilization of

similarity equations and thermophysical models of conventional and hybrid nanofluids. Thereafter, the model is analyzed systematically through a numerical technique and the results furnished for the parameters involved determined that:

- The movement of $[(Al_2O_3\text{-}Fe_3O_4)/blood]_{hnf}$ and $[(Al_2O_3)/blood]_{nf}$ could be controlled against the high strength of the magnetic field which is beneficial for industrial applications.
- The stretching parameter is useful for rapid movement of the nanofluids over a 3D surface.
- The heat transmission ability of $[(Al_2O_3\text{-}Fe_3O_4)/blood]_{hnf}$ due to the radiated surface is much higher than $[(Al_2O_3)/blood]_{nf.}$
- The % volume concentration is a core factor in hybrid and common liquids particularly in the heat storage ability.
- The skin friction and Nusselt number upsurge by intensifying the strength of the magnetic field and thermal radiations, respectively.
- The interaction of oxide nanomaterials with blood as presented in the study will contribute potentially in the field of medical and biomedical engineering.

Data availability statement

The raw data supporting the conclusions of this article will be made available by the authors, without undue reservation. The data will be provided upon reasonable request.

Author contributions

All authors listed have made a substantial, direct, and intellectual contribution to the work and approved it for publication. Adnan and WA wrote original draft, UK done mathematical analysis, KG, ZR, EE, and ME-S potentially contributed revision, language editing and study validation.

Funding

Conflict of interest

The authors declare that the research was conducted in the absence of any commercial or financial relationships that could be construed as a potential conflict of interest.

Publisher's note

All claims expressed in this article are solely those of the authors and do not necessarily represent those of their affiliated organizations, or those of the publisher, the editors, and the reviewers. Any product that may be evaluated in this article, or claim that may be made by its manufacturer, is not guaranteed or endorsed by the publisher.

References

Abbasi, A., Ahmed, N., and Mohyud-Din, S. T. (2017). Flow of Magneto-Nanofluid over a Thermally Stratified Bi-directional Stretching Sheet in the Presence of Ohmic Heating: A Numerical Study of Particle Shapes. *Eng. Comput. Swans.* 34 (8), 2499–2513. doi:10.1108/ec-04-2017-0127

Adnan, and Ashraf, W. (2022a). Numerical Thermal Featuring in γAl_2O_3-$C_2H_6O_2$ Nanofluid under the Influence of Thermal Radiation and Convective Heat Condition by Inducing Novel Effects of Effective Prandtl Number Model (EPNM). *Adv. Mech. Eng.* 14, 168781322211065. doi:10.1177/16878132221106577

Adnan, and Ashraf, W. (2022b). Thermal Efficiency in Hybrid (Al_2O_3-CuO/H_2O) and Ternary Hybrid Nanofluids (Al_2O_3-CuO-Cu/H_2O) by Considering the Novel Effects of Imposed Magnetic Field and Convective Heat Condition. *Waves Random Complex Media.* doi:10.1080/17455030.2022.2092233

Adnan, S. Z. A., Khan, U., Abdeljawad, T., Ahmed, N., Khan, I., Nisar, K. S., et al. (2020). Investigation of Thermal Transport in Multi-Shaped Cu Nanomaterial-Based Nanofluids. *Materials* 13, 2737. doi:10.3390/ma13122737

Adnan, S. Z. A., Zaidi, U., Khan, N., Ahmed, Y., Chu, M., Khan, I., et al. (2020). Impacts of Freezing Temperature Based Thermal Conductivity on the Heat Transfer Gradient in Nanofluids: Applications for a Curved Riga Surface. *Molecules* 25, 2152. doi:10.3390/molecules25092152

Adnan, Khan, U., and Ahmed, N. (2022). Thermal Enhancement and Entropy Investigation in Dissipative ZnO-SAE50 under Thermal Radiation: a Computational Paradigm. *Waves Random Complex Media.* doi:10.1080/17455030.2022.2053243

Adnan, W. A., Andualem, M., and Khan, I. (2022). Thermal Transport Investigation and Shear Drag at Solid–Liquid Interface of Modified Permeable Radiative-SRID Subject to Darcy–Forchheimer Fluid Flow Composed by γ-nanomaterial. *Sci. Rep.* 12, 3564. doi:10.1038/s41598-022-07045-2

Adnan, W. Ashraf, Alghtani, A. H., Khan, I., and Andualem, M. (2022). Thermal Transport in Radiative Nanofluids by Considering the Influence of Convective Heat Condition. *J. Nanomater.* 2022, 1–11. doi:10.1155/2022/1854381

Ahmed, N., Abbasi, A., Saba, F., and Mohyud-Din, S. T. (2018). Flow of Ferro-Drmagnetic Nanoparticles in a Rotating System: a Numerical Investigation of Particle Shapes. *Indian J. Phys.* 92, 969–977. doi:10.1007/s12648-018-1186-4

Ahmed, N., Adnan, Khan, U., and Mohyud-Din, S. T. (2017). Influence of Thermal Radiation and Viscous Dissipation on Squeezed Flow of Water between Riga Plates Saturated with Carbon Nanotubes. *Colloids Surfaces A Physicochem. Eng. Aspects* 522, 389–398. doi:10.1016/j.colsurfa.2017.02.083

Ahmed, N., Adnan, Khan, U., and Mohyud-Din, S. T. (2020). Hidden Phenomena of MHD on 3D Squeezed Flow of Radiative-H_2O Suspended by Aluminum Alloys Nanoparticles, *Eur. Phys. J. Plus* 135, 875. doi:10.1140/epjp/s13360-020-00870-2

Akbar, N. S., Maraj, E. N., Noor, N. F. M., and Habib, M. B. (2022). Exact Solutions of an Unsteady Thermal Conductive Pressure Driven Peristaltic Transport with Temperature-dependent Nanofluid Viscosity. *Case Stud. Therm. Eng.* 35, 102124. doi:10.1016/j.csite.2022.102124

Akram, J., Akbar, N. S., Alansari, M., and Tripathi, D. (2022). Electroosmotically Modulated Peristaltic Propulsion of TiO2/10W40 Nanofluid in Curved Microchannel. *Int. Commun. Heat Mass Transf.* 136, 106208. doi:10.1016/j.icheatmasstransfer.2022.106208

Akram, J., and Akbar, N. S. (2020). Biological Analysis of Carreau Nanofluid in an Endoscope with Variable Viscosity. *Phys. Screen.* 95, 055201–055205. doi:10.1088/1402-4896/ab74d7

Akram, J., Akbar, N. S., and Maraj, E. (2020). Chemical Reaction and Heat Source/sink Effect on Magnetonano Prandtl-Eyring Fluid Peristaltic Propulsion in an Inclined Symmetric Channel. *Chin. J. Phys.* 65, 300–313. doi:10.1016/j.cjph.2020.03.004

Akram, J., Akbar, N. S., and Tripathi, D. (2022). Analysis of Electroosmotic Flow of Silver-Water Nanofluid Regulated by Peristalsis Using Two Different Approaches for Nanofluid. *J. Comput. Sci.* 62, 101696. doi:10.1016/j.jocs.2022.101696

Akram, J., Akbar, N. S., and Tripathi, D. (2022). Electroosmosis Augmented MHD Peristaltic Transport of SWCNTs Suspension in Aqueous Media. *J. Therm. Anal. Calorim.* 147, 2509–2526. doi:10.1007/s10973-021-10562-3

Akram, J., Akbar, N. S., and Tripathi, D. (2022). Entropy Generation in Electroosmotically Aided Peristaltic Pumping of MoS2 Rabinowitsch Nanofluid. *Fluid Dyn. Res.* 54, 15507–15511. doi:10.1088/1873-7005/ac4e7b

Akram, J., Akbar, N. S., and Tripathi, D. (2022). Thermal Analysis on MHD Flow of Ethylene Glycol-Based BNNTs Nanofluids via Peristaltically Induced Electroosmotic Pumping in a Curved Microchannel. *Arab. J. Sci. Eng.* 47, 7487–7503. doi:10.1007/s13369-021-06173-7

Alharbi, K. A. M., Khan, U., Ahammad, N. A., Adnan, Ullah, B., Wahab, H. A., et al. (2022). Heat Transport Mechanism in Cu/water and (Cu–Al2O3)/water under the Influence of Thermophysical Characteristics and Non-linear Thermal Radiation for Blasius/Sakiadis Models: Numerical Investigation. *J. Indian Chem. Soc.* 99, 100578–8. doi:10.1016/j.jics.2022.100578

Alshare, A., Al-Kouz, W., and Khan, W. (2020). Cu-Al2O3Water Hybrid Nanofluid Transport in a Periodic Structure. *Processes* 8 (3), 285. doi:10.3390/pr8030285

Ashraf, W., Al-Johani, A. S., Khan, I., Andualem, M., Ahmed, N., Mohyud-Din, S. T., et al. (2022). Impact of Freezing Temperature (Tfr) of Al_2O_3 and Molecular Diameter ($H_2O)_d$ on Thermal Enhancement in Magnetized and Radiative Nanofluid with Mixed Convection. *Sci. Rep.* 12, 703. doi:10.1038/s41598-021-04587-9

Butt, A. W., Akbar, N. S., and Mir, N. A. (2020). Heat Transfer Analysis of Peristaltic Flow of a Phan-Thien-Tanner Fluid Model Due to Metachronal Wave of Cilia. *Biomech. Model. Mechanobiol.* 19 (5), 1925–1933. doi:10.1007/s10237-020-01317-4

Colak, A. B., Yildiz, O., Bayrak, M., and Tezekici, B. S. (2020). Experimental Study for Predicting the Specific Heat of Water Based Cu-Al2O3 Hybrid Nanofluid Using Artificial Neural Network and Proposing New Correlation. *Int. J. Energy Res.* 44 (9), 7198–7215. doi:10.1002/er.5417

Devi, S. P. A., and Devi, S. S. U. (2016). Numerical Investigation of Hydromagnetic Hybrid Cu–Al2O3/Water Nanofluid Flow over a Permeable Stretching Sheet with Suction. *Int. J. Nonlinear Sci. Numer. Simul.* 17 (5), 249–257. doi:10.1515/ijnsns-2016-0037

Devi, S. U., and Devi, S. P. A. (2016). Numerical Investigation on Three Dimensional Hybrid Cu–Al2O3/Water Nanofluid Flow over a Stretching Sheet with Effecting Lorentz Force Subject to Newtonian Heating. *Can. J. Phys.* 94, 490–496. doi:10.1139/cjp-2015-0799

Habib, M. B., and Akbar, N. S. (2021). New Trends of Nanofluids to Combat *Staphylococcus aureus* in Clinical Isolates. *J. Therm. Anal. Calorim.* 143, 1893–1899. doi:10.1007/s10973-020-09502-4

Hayat, T., Imtiaz, M., Alsaedi, A., and Kutbi, M. A. (2015). MHD Three-Dimensional Flow of Nanofluid with Velocity Slip and Nonlinear Thermal Radiation. *J. Magnetism Magnetic Mater.* 396, 31–37. doi:10.1016/j.jmmm.2015.07.091

Hosseinzadeh, K., Asadi, A., Mogharrebi, A. R., Azari, M. E., and Ganji, D. D. (2021). Investigation of Mixture Fluid Suspended by Hybrid Nanoparticles over Vertical Cylinder by Considering Shape Factor Effect. *J. Therm. Anal. Calorim.* 143, 1081–1095. doi:10.1007/s10973-020-09347-x

Jamaludin, A., Naganthran, K., Nazar, R., and Pop, I. (2020). MHD Mixed Convection Stagnation-point Flow of Cu-Al2O3/water Hybrid Nanofluid over a Permeable Stretching/shrinking Surface with Heat Source/sink. *Eur. J. Mech. - B/Fluids* 84, 71–80. doi:10.1016/j.euromechflu.2020.05.017

Jamshad, W., Devi, S. U., Boukili, A., Nisar, K. S., Sooppy Nisar, K., Zakarya, M., et al. (2021). Evaluating the Unsteady Casson Nanofluid over a Stretching Sheet with Solar Thermal Radiation: An Optimal Case Study. *Case Stud. Therm. Eng.* 26, 101160–101210. doi:10.1016/j.csite.2021.101160

Javid, K., Hassan, M., Tripathi, D., Khan, S., Bobescu, E., and Bhatti, M. M. (2021). Double-diffusion Convective Biomimetic Flow of Nanofluid in a Complex Divergent Porous Wavy Medium under Magnetic Effects. *J. Biol. Phys.* 47, 477–498. doi:10.1007/s10867-021-09583-8

Kashi, N. S., Arifin, N. M., Pop, L., Nazar, R., Hafidzuddin, E. H., and Wahi, N. (2020). Three-Dimensional Hybrid Nanofluid Flow and Heat Transfer Past a Permeable Stretching/Shrinking Sheet with Velocity Slip and Convective Condition. *Chin. J. Phys.* 66, 157–171. doi:10.1016/j.cjph.2020.03.032

Khan, U., Abbasi, A., Ahmed, N., and Mohyud-Din, S. T. (2017). Particle Shape, Thermal Radiations, Viscous Dissipation and Joule Heating Effects on Flow of Magneto-Nanofluid in a Rotating System. *Eng. Comput. Swans.* 34 (8), 2479–2498. doi:10.1108/ec-04-2017-0149

Khan, U., Adnan, and Haleema, B. (2022). Thermal Performance in Nanofluid and Hybrid Nanofluid under the Influence of Mixed Convection and Viscous Dissipation: Numerical Investigation. *Waves Random Complex Media*. doi:10.1080/17455030.2022.2036389

Khan, U., Ullah, B., Wahab, H. A., Ullah, I., Almuqrin, M. A., and Khan, I. (2022). Comparative Thermal Transport Mechanism in Cu-H$_2$o and Cu- Al$_2$O$_3$/H2O Nanofluids: Numerical Investigation. *Waves Random Complex Media*. doi:10.1080/17455030.2021.2023783

Khan, W., Khan, I., Fayz-Al-Asad, M., and Adnan (2021). Applied Mathematical Modelling and Heat Transport Investigation in Hybrid Nanofluids under the Impact of Thermal Radiation: Numerical Analysis. *Math. Problems Eng.* 1, 10. doi:10.1155/2021/2180513

Khashi, N, S., Arifin, N, M., and Pop, I. (2020). Mixed Convective Stagnation Point Flow towards a Vertical Riga Plate in Hybrid Cu- Al$_2$O$_3$/Water Nanofluid. *Mathematics* 8 (6), 912. doi:10.3390/math8060912

Khashi, N. S., Arifin, N. M., Pop, I., Nazar, R., and Hafidzuddin, E. H. (2021). A New Similarity Solution with Stability Analysis for the Three-Dimensional Boundary Layer of Hybrid Nanofluids. *Int. J. Numer. Methods Heat. Fluid Flow.* 31 (9), 809–828. doi:10.1108/hff-04-2020-0200

Leong, L. S., Basie, M. F. M., Jaafar, N. A., Chaharborj, S. S., Khairuddin, T. K. A., and Naganthran, K. (2020). Numerical Solutions for the Thin Film Hybrid Nanofluid Flow and Heat Transfer over an Unsteady Stretching Sheet. *Open J. Sci. Technol.* 3, 4..

Lund, L. A., Omar, Z., Dero, S., Khan, I., Baleanu, D., and Nisar, K. S. (2020). Magnetized Flow of Cu+ Al$_2$O$_3$+ H$_2$O Hybrid Nanofluid in Porous Medium: Analysis of Duality and Stability. *Symmetry* 12 (9), 1513. doi:10.3390/sym12091513

Lund, L. A., Omar, Z., Khan, I., Seikh, A. H., Sherif, E. S. M., and Nasir, A. S. (2019). Stability Analysis and Multiple Solution of Cu–Al$_2$O$_3$/H2O Nanofluid Contains Hybrid Nanomaterials over a Shrinking Surface in the Presence of Viscous Dissipation. *J. Mater. Res. Technol.* 9 (1), 421–432. doi:10.1016/j.jmrt.2019.10.071

Mehryan, S. A. M., Kashkooli, F. M., Ghalambaz, M., and Chamkha, A. (2017). Free Convection of Hybrid Al$_2$O$_3$-Cu Water Nanofluid in a Differentially Heated Porous Cavity. *Adv. Powder Technol.* 28 (9), 2295–2305. doi:10.1016/j.apt.2017.06.011

Prakash, M., Devil, S., and Uma, S. (2016). Hydromagnetic Hybrid Al$_2$O$_3$-Cu/Water Nanofluid Flow over a Slendering Stretching Sheet with Prescribed Surface Temperature. *Asian J. Res. Soc. Sci. humanit.* 6 (9), 1921–1936. doi:10.5958/2249-7315.2016.00915.1

Roy, N. C., Saha, L. K., and Sheikholeslami, M. (2020). Heat Transfer of a Hybrid Nanofluid Past a Circular Cylinder in the Presence of Thermal Radiation and Viscous Dissipation. *AIP Adv.* 10 (9), 095208.

Sajid, T., Jamshed, W., Shahzad, F., Boukili, A. E., Ez-Zahraouy, H., Nisar, K. S., et al. (2021). Study on Heat Transfer Aspects of Solar Aircraft Wings for the Case of Reiner-Philippoff Hybrid Nanofluid Past a Parabolic Trough: Keller Box Method. *Phys. Screen.* 96, 095220–095229. doi:10.1088/1402-4896/ac0a2a

Saleem, N., Munawar, S., and Tripathi, D. (2021). Entropy Analysis in Ciliary Transport of Radiated Hybrid Nanofluid in Presence of Electromagnetohydrodynamics and Activation Energy. *Case Stud. Therm. Eng.* 28, 101665. doi:10.1016/j.csite.2021.101665

Sridhar, V., Ramesh, K., Tripathi, D., and Vivekanand, V. (2022). Analysis of Thermal Radiation, Joule Heating, and Viscous Dissipation Effects on Blood-Gold Couple Stress Nanofluid Flow Driven by Electroosmosis. *Heat. Trans.* 51, 4080–4101. doi:10.1002/htj.22490

Takabi, B., and Shokouhmand, H. (2015). Effects of Al$_2$O$_3$–Cu/water Hybrid Nanofluid on Heat Transfer and Flow Characteristics in Turbulent Regime. *Int. J. Mod. Phys. C* 26, 1550047. doi:10.1142/S0129183115500473

Tripathi, D., Jayavel, P., Osman, A. B., and Srivastava, V. (2022). EMHD Casson Hybrid Nanofluid Flow over an Exponentially Accelerated Rotating Porous Surface. *J. Porous Media*. doi:10.1615/JPorMedia.2022041050

Tripathi, D., Prakash, J., Reddy, M. G., and Kumar, R. (2021). Numerical Study of Electroosmosis-Induced Alterations in Peristaltic Pumping of Couple Stress Hybrid Nanofluids through Microchannel. *Indian J. Phys.* 95, 2411–2421. doi:10.1007/s12648-020-01906-0

Usman, M., Zubair, T., Haq, R., and Wang, W. (2018). Cu-Al$_2$O$_3$/Water Hybrid Nanofluid through a Permeable Surface in the Presence of Nonlinear Radiation and Variable Thermal Conductivity via LSM. *Int. J. Heat Mass Transf.* 126, 1347–1356. doi:10.1016/j.ijheatmasstransfer.2018.06.005

Wahid, N. S., Arifin, N. M., Turkyilmazoglu, M., Hafidzuddin, M. E. H., and Rahmin, N. A. A. (2020). MHD Hybrid Cu-Al2O3/Water Nanofluid Flow with Thermal Radiation and Partial Slip Past a Permeable Stretching Surface: Analytical Solution. *JNanoR.* 64, 75–91. doi:10.4028/www.scientific.net/jnanor.64.75

Waqas, H., Farooq, U., Alghamdi, M., Muhammad, T., and Alshomrani, A. S. (2021). On the Magnetized 3D Flow of Hybrid Nanofluids Utilizing Nonlinear Radiative Heat Transfer. *Phys. Screen.* 96 (9), 095202. doi:10.1088/1402-4896/ac0272

Zaina, N. K., Nazar, R., Naganthran, K., and Pop, I. (2020). Impact of Anisotropic Slip on the Stagnation-point Flow Past a Stretching/shrinking Surface of the Al$_2$O$_3$-Cu/H$_2$O Hybrid Nanofluid. *Appl. Math. Mech.* 41, 1401–1416. doi:10.1007/s10483-020-2642-6

Zainal, N. A., Nazar, R., and Naganthran, K., (2021). Unsteady MHD Mixed Convection Flow in Hybrid Nanofluid at Three-Dimensional Stagnation Point, *Mathematics* 9, doi:10.3390/math9050549